Mon. Not. R. Astron. Soc. **268**, 276–290 (1994)

A submillimetre continuum survey of pre-protostellar cores

D. Ward-Thompson,[1] P. F. Scott,[2] R. E. Hills[2] and P. André[3]

[1]*Royal Observatory, Blackford Hill, Edinburgh EH9 3HJ*
[2]*Mullard Radio Astronomy Observatory, Cavendish Laboratory, Madingley Road, Cambridge CB3 0HE*
[3]*Service d'Astrophysique, Centre d'Etudes de Saclay, F-91191 Gif-sur-Yvette Cedex, France*

Accepted 1993 December 20. Received 1993 December 17; in original form 1993 November 19

ABSTRACT

Results are presented of a submillimetre continuum survey of 21 Myers cores that have no known infrared (near-IR or *IRAS*) associations – the so-called 'starless cores'. ^{13}CO maps show that 17 of the cores have structure in the form of one or more clumps, with significant departures from spherical symmetry. The clumps were surveyed in the submillimetre continuum, but only 12 were detected. In all cases no more than one clump in each of the Myers cores was detected in the continuum, no matter how many ^{13}CO clumps it contained. Five of the clumps were mapped in the continuum, to demonstrate that they are true emission peaks. The continuum peaks are not always exactly coincident with the ^{13}CO peaks, indicating that the ^{13}CO may be optically thick. For the first time a size difference is found between the starless cores and the cores with *IRAS* sources: the continuum clumps in the centres of starless cores are all less centrally peaked and more diffuse than the equivalent continuum clumps previously found in Myers cores with *IRAS* sources. Nevertheless, the starless cores are more centrally condensed than a constant-density sphere. Mass and density estimates show that the continuum peaks are true density peaks, of $\sim 10^5$–10^6 cm^{-3}. Photometry of the clumps shows that they have insufficient bolometric luminosities to be consistent with the earliest phase of accreting protostars predicted by the Standard Protostellar Model. The lifetimes of the clumps derived from statistical considerations are shown to be too long for the cores to be undergoing free-fall collapse, but are consistent with ambipolar diffusion time-scales. All of the clumps are found to have masses close to their virial masses, as expected during the quasi-static ambipolar diffusion phase. The starless cores with submillimetre continuum detections are therefore hypothesized to be pre-protostellar in nature, and sites of future star formation. However, none of the mapped clumps shows the steep, $\rho(r) \propto r^{-2}$, power-law radial density profile predicted by the Standard Protostellar Model. All have profiles that flatten out near their centres. This means either that the cores have not yet reached this stage in their evolution, or that cores do not achieve such steep density profiles prior to star formation, due to support by some other mechanism, such as a magnetic field. Previous observations may have failed to observe this flattening, due to their lower angular resolution. The radial profiles of the continuum clumps are, however, consistent with those predicted by a more recent theory of magnetic support of cores during ambipolar diffusion.

Key words: stars: formation – ISM: clouds – dust, extinction – ISM: molecules – radio continuum: ISM.

1 INTRODUCTION

1.1 The observational sample

Low-mass star formation is known to occur within dark clouds, where density inhomogeneities caused by random motions lead to the formation of cores within a cloud. The most extensive survey so far carried out of cold cores within dark clouds is that of Myers and co-workers (Myers, Linke & Benson 1983, hereafter MLB; Myers & Benson 1983, hereafter MB; Myers et al. 1987; Benson & Myers 1989, hereafter BM). MLB selected 90 positions of high visual opacity on the Palomar Observatory Sky Survey (POSS) plates, and surveyed them in ^{13}CO and C^{18}O (both are column density tracers), while MB surveyed them in NH_3 (tracer of high density). BM reported a larger survey of a total of 149 positions, of which they detected NH_3 at 78 positions. All of these surveys were carried out at intermediate resolution (~1–2 arcmin). These regions of high density within dark clouds are commonly known as 'Myers cores' and are prime candidates for star-forming cores.

The *IRAS* all-sky survey was searched for associations with the ~90 cores (Beichman et al. 1986) and around half were found to have associated *IRAS* sources. Of these *IRAS* sources, some two-thirds have no optical counterpart, while around one-third are associated with T Tauri stars (TTSs). Beichman et al. therefore deduced that the invisible *IRAS* sources must be either embedded TTSs or objects at an earlier stage of evolution. The only statistical difference (at the 3σ level) in the properties of the cores with *IRAS* sources, compared to those without, is the mean linewidth (Beichman et al. 1986). It was therefore hypothesized that the cores with *IRAS* sources have already formed young stellar objects (YSOs) at their centres, whose stellar winds disrupt the surrounding material, broadening the observed lines, while those without *IRAS* sources were designated 'starless cores'.

Millimetre and submillimetre continuum studies have been carried out of the cores with *IRAS* sources (Walker, Adams & Lada 1990; Ladd et al. 1991a,b; André & Montmerle 1994), and in some instances their spectral energy distributions seem to agree with the model predictions for the case where a central object has formed and the energy released by the accretion process is appearing as far-IR and submillimetre emission (e.g. L1527 – Ladd et al. 1991a). Less work has been done on the cores with no *IRAS* sources. A few of the cores were detected at 350 μm at low resolution, and a few 1.3-mm upper limits were derived, by Mezger, Sievers & Zylka (1991). However, no detailed survey has been carried out of the continuum emission from cores without *IRAS* sources.

In this paper we present the results of a comprehensive submillimetre continuum study of Myers cores with no associated *IRAS* sources, and we attempt to define their evolutionary status.

1.2 Protostars and pre-protostellar cores

Hydrostatic equilibrium is possible for a given core provided that a certain critical mass is not exceeded (Shu 1977, and references therein). When this condition is no longer satisfied, inside-out collapse sets in, with the innermost part of the core collapsing first, and a collapse expansion wave (CEW) propagating outwards from the centre at the local sound speed (Larson 1969; Shu 1977). At the very beginning of the collapse, the heat generated by the compressional work of the gravitational forces is freely radiated away, and the cloud core stays isothermal. However, the increase in density is such that a hydrostatic, opaque stellar object soon forms at the centre, and starts heating up, while continuing to accrete material from a surrounding in-falling envelope. For the purposes of this paper, we will follow Adams, Lada & Shu (1987 – hereafter ALS) and define a protostar as this hydrostatic, condensed object which will eventually become a star. Initially, most of the mass of the protostellar system is in the cloud core and envelope rather than in the central protostar, which contains only a small fraction of its final, main-sequence mass. By the time the CEW reaches the outer edge of the cloud core, roughly half of the mass within it will have accreted on to the central protostar (Beichman et al. 1986). When the protostar has accumulated most of the core mass, it becomes a pre-main-sequence star which evolves approximately at fixed mass.

The location and identification of protostars observationally are very difficult, partly due to the fact that, by their very nature, protostars are found in extremely obscured regions, and partly because the infrared properties of accreting protostars are not dissimilar to those of the far more evolved contracting T Tauri stars, when the latter are deeply embedded in cloud cores (Beichman et al. 1986). Initial claims that the infrared Class I sources were protostars (ALS) have been disputed on statistical grounds. For example, Wilking, Lada & Young (1989), in a survey of the young stellar cluster in ρ Ophiuchi, found that roughly one-third of all the embedded sources were Class I, while Stahler & Fletcher (1991) predicted that only ~ 1 per cent of embedded sources in a young stellar cluster should be protostars. Furthermore, André & Montmerle (1994) showed that the Class I sources in ρ Oph are in general surrounded by no more than 0.1 $M_\odot$ of circumstellar material, suggesting that these objects have already accumulated most of their final mass, and are already at the end of their protostellar evolution.

Better candidate protostars have recently been identified by André, Ward-Thompson & Barsony (1993 – hereafter AWB), who classified a number of sources that have little or no infrared emission, but are very luminous in the submillimetre and radio regions. These sources were denoted Class 0 by AWB to signify their extreme youth, and were hypothesized to be genuine protostars. The prototype member of this new class is the bipolar outflow source VLA1623 (AWB, and references therein), although other sources had previously been discovered that were seen to have similar properties, such as NGC1333-IRAS4 (Sandell et al. 1991), L1527 (Ladd et al. 1991a) and B335 (Chandler et al. 1990; Zhou et al. 1993).

The submillimetre continuum source ρ Oph–SM1 (hereafter SM1), which was originally discovered by Ward-Thompson et al. (1989), was identified by AWB as being at an even earlier evolutionary stage than VLA1623 and other Class 0 sources, on the grounds that it is more diffuse and less centrally condensed, and does not have a bipolar outflow or compact VLA emission. AWB hypothesized that SM1 could in fact be pre-protostellar in nature, and the prototype of a still earlier class of source.

Recently, Chini et al. (1993) have detected a similarly strong submillimetre source in Orion (HH24MMS), which is a good candidate for being in the initial, isothermal phase of protostellar collapse, on the grounds that it is apparently gravitationally unstable but has not yet formed a central stellar object. If this is true, HH24MMS would be at an evolutionary stage intermediate between SM1 and VLA1623.

Thus an empirical picture appears to be emerging for an evolutionary sequence from cold molecular core to T Tauri star. However, it is not possible to build a comprehensive model of the earliest phases of this evolution from the small number of objects presently known at these stages. It was therefore decided to undertake a submillimetre continuum survey of cloud cores, to search for more examples of HH24MMS-, SM1- and VLA1623-type objects, and to attempt to classify the cores into a more complete evolutionary sequence.

The paper is laid out as follows: Section 2 describes the observations that were made; the results are presented in Section 3; Section 4 details the physical parameters that can be derived from the data; Section 5 discusses the evolutionary sequence of the cores; and Section 6 outlines the main conclusions of the paper.

2 OBSERVATIONS

Submillimetre continuum observations at 450, 800 and 1100 μm were carried out at the James Clerk Maxwell Telescope (JCMT), located on Mauna Kea, Hawaii, on the evenings of 1991 December 27 to 1992 January 2, 17:30–01:30 HST (UT = 03:30–11:30), on the mornings of 1992 September 23 to 29, 01:30–09:30 HST (UT = 11:30–19:30), and on the mornings of 1993 March 2 to 8, 01:30–09:30 HST (UT = 11:30–19:30). The detector used was the common-user receiver UKT14, which contains a single-element, ^{3}He-cooled Ge:In:Sb bolometer, and a series of filters matched to the atmospheric transmission windows (Duncan et al. 1990). The observations were carried out while using the secondary mirror to chop in azimuth at around 7 Hz and synchronously to detect the signal, thus rejecting 'sky' emission.

Calibration was performed during the first run by initially mapping the planets Uranus and Mars (brightness temperatures taken from Orton et al. 1986 and Griffin & Orton 1993), to measure the detector sensitivity at each waveband, during the afternoon of 1991 December 28, 13:30–16:30 HST. During this time, estimates were obtained of the atmospheric opacity in all wavebands, based on the monitoring of the opacity at 225 GHz provided by the NRAO 'tipper' radiometer located at the adjacent Caltech Submillimeter Observatory (CSO), using standard ratios (e.g. AWB). Subsequent monitoring of secondary calibration sources of known intensity, together with continuous monitoring of the 225-GHz opacity, allowed the atmospheric opacity, τ, to be calculated at all times, in all wavebands.

The secondary calibrators used were the strong submillimetre sources W3(OH) and CRL618 (Sandell, private communication), which were measured in all wavebands at least once per hour. The opacities derived using W3(OH) and CRL618 as monitors gave results consistent with the values for τ determined using the radiometer measurements. During the second run the CSO radiometer was not available for the first three nights due to a lightning strike. Thus the detector sensitivities and atmospheric opacities had to be estimated from the calibrators alone in the first instance. In addition to Mars, W3(OH) and CRL618, the additional calibrator NGC2071(IR) was also used, and a fully self-consistent calibration was obtained. This was verified with the radiometer measurements when it was repaired, and gave consistent results. During the third run the same technique was employed as for the first run, this time using the planet Uranus as the primary calibrator (Orton et al. 1986; Griffin & Orton 1993), and IRAS16293-2422 as a secondary calibrator (Walker et al. 1986; Sandell, private communication). Altogether, we estimate our total absolute calibration uncertainty to be ~20 per cent at 1100 μm and 800 μm, and ~30–40 per cent at 450 μm.

The 450-μm atmospheric transmission at zenith was good (~40 per cent) and very stable throughout most of the first run (typical of good conditions at the site). The 800-μm zenith transmission was ~80 per cent and the 1100-μm zenith transmission was ~90 per cent during this time. During the second run the 450-μm atmospheric transmission at zenith varied from ~10–30 per cent (typical of more average conditions), and the 800- and 1100-μm transmissions were correspondingly lower, and consequently the longer wavelength observations were emphasized. During the third run the conditions were again good, with 450-μm zenith transmission as high as 50 per cent at times. Pointing and focus checks were performed typically once per hour during all runs. The focus was found to be very stable throughout, and the pointing was observed to be accurate to better than 3 arcsec (maximum total deviation observed).

Millimetre line observations were carried out at JCMT during the above periods using the common-user Schottky heterodyne receiver A2 (Davies et al. 1992). Measurements were made of the ^{13}CO ($J = 2 \rightarrow 1$) transition at a frequency of 220.398 GHz. The beamsize at this frequency is ~20 arcsec. Grid mapping was performed, with calibration being carried out using the receiver's internal hot- and cold-load system. The channel width was 0.3 km s^{-1}, and the typical system temperature was ~400 K. After simple baseline subtraction had been carried out, no further data reduction was found to be necessary. The final noise per channel in the reduced maps was typically ~0.1 K rms.

Millimetre continuum observations were carried out at 1.3 mm using the IRAM 30-m telescope located at Pico Veleta, Spain, during the period 1992 November 27 to December 1, 20:00–05:00 UT. The detector used was the IRAM facility single-channel bolometer (Thum et al. 1992) during its first scheduled period of observations on the telescope. Calibration was made using the planet Mars to measure detector sensitivity, as described above. The atmospheric opacity was measured by performing regular 'skydips' with the telescope, in the standard fashion. The zenith transmission varied from roughly 80 per cent to about 90 per cent during the first three nights, but was considerably worse during the last night, when no significant observations were made. We estimate our total absolute calibration uncertainty to be ~20 per cent at 1.3 mm.

1.3-mm continuum observations were also carried out at the SEST 15-m telescope in La Silla, Chile, with the common-user bolometer built by MPIfR, as part of another project, scheduled during the evenings of 1993 September 8, 10 and 11 (20:00–03:00 UT). Calibration was performed through ON-OFF and mapping observations of the planet Uranus. The beamsize was measured to be 24 arcsec. Chopping was provided by a focal-plane chopper operating at 4.5 Hz with a throw of about 70 arcsec in azimuth. The (zenith) atmospheric transmission was monitored using the same skydip method as at IRAM and was found to be ~80 per cent throughout the period of the observations.

3 RESULTS

Myers cores without *IRAS* sources were selected from the list of Beichman et al. (1986), and their positions were taken from BM, who divided their sources into those that have D <500 pc, and those that have D >500 pc, or have indeterminate distance. We concentrated mainly on the nearer sources.

Initially, photometry was carried out at the BM positions. However, due to the relatively large beam of the BM observations (~1.5 arcmin), the accuracy of their peak positions is limited. It was therefore subsequently deemed necessary to ascertain more accurate positions.

Time constraints and the weakness of the sources made it impossible to map each entire core in the submillimetre continuum, since typical integration times on the peaks alone were a minimum of ~5 min per point in good weather, and each core covers several square arcmin. Therefore an observing

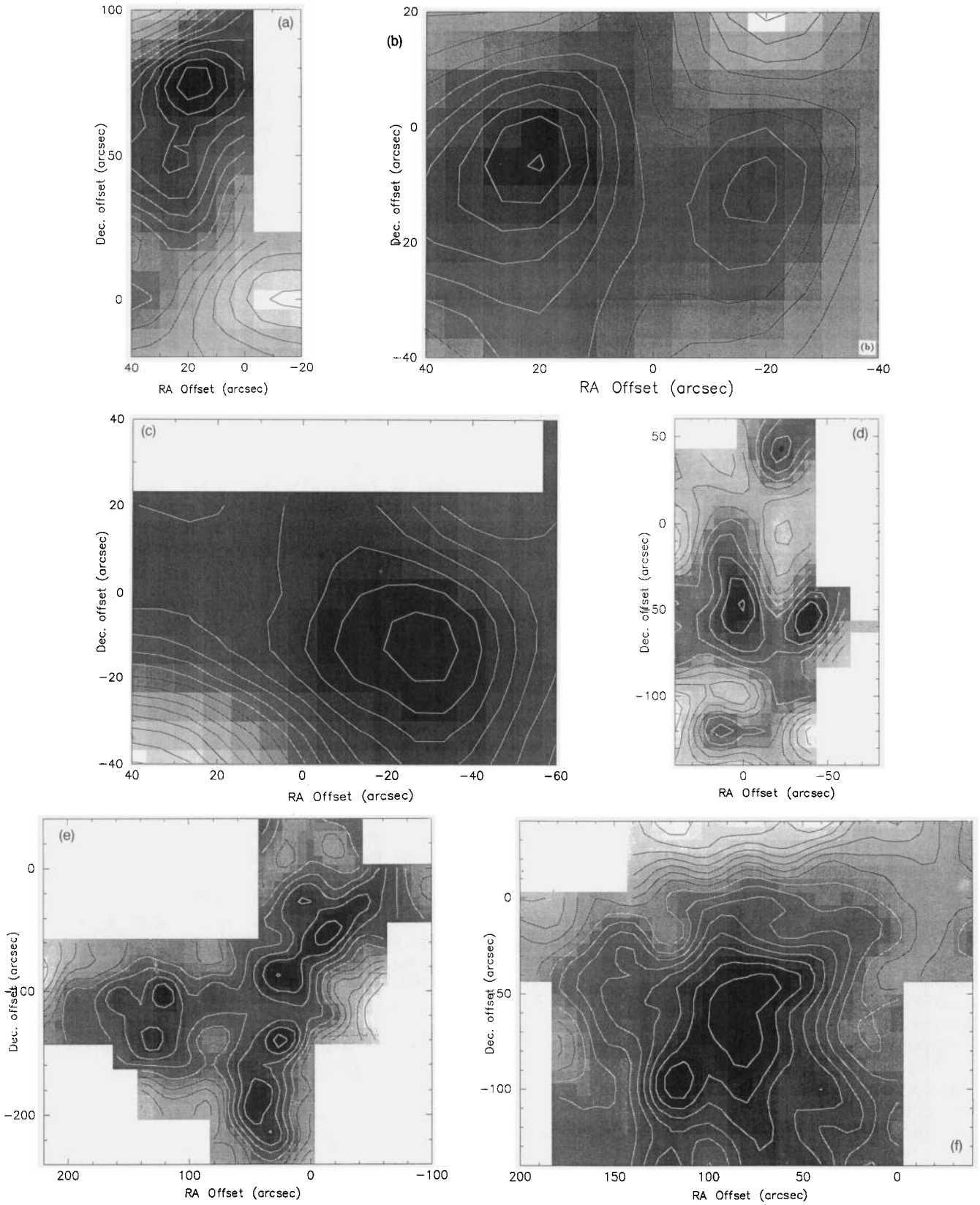

Figure 1. 'Finding charts'. Grey-scale images, with contour maps superposed, of integrated ^{13}CO (2→1) emission from six of the starless cores. RA and Dec. offsets are marked in arcsec. (a) L1506, map origin is at RA (1950) = $04^h15^m29^s$, Dec. (1950) = +25°12′10″, base contour level is 0.65 K km s^{-1}, contour interval is 0.05 K km s^{-1}. (b) L1544, map origin is at RA (1950) = $05^h01^m14^s$, Dec. (1950) = +25°07′00″, base contour level is 1.9 K km s^{-1}, contour interval is 0.1 K km s^{-1}. (c) L1582A, map origin is at RA (1950) = $05^h29^m16^s$, Dec. (1950) = +12°28′20″, base contour level is 1.5 K km s^{-1}, contour interval is 0.5 K km s^{-1}. (d) L1696A, map origin is at RA (1950) = $16^h25^m30^s$, Dec. (1950) = −24°12′32″, base contour level is 7.25 K km s^{-1}, contour interval is 0.25 K km s^{-1}. (e) L1689A, map origin is at RA (1950) = $16^h29^m10^s$, Dec. (1950) = −24°56′32″, base contour level is 9.0 K km s^{-1}, contour interval is 1.0 K km s^{-1}. (f) L1689B, map origin is at RA (1950) = $16^h31^m40^s$, Dec. (1950) = −24°30′00″, base contour level is 2.75 K km s^{-1}, contour interval is 0.25 K km s^{-1}.

Table 1. Source list. Column 1 gives the source names designated by BM. Columns 2 and 3 list the RA (1950) and Dec. (1950) of the positions searched for NH_3 by BM. Columns 4 and 5 list the positions at which continuum photometry was carried out (in some cases these are offset slightly from the ^{13}CO peak position). If more than one peak was found in ^{13}CO, only positions with continuum detections are listed. In no core was more than one continuum peak found. Columns 6–9 list the source flux densities in mJy in a 12-arcsec beam at 1300 μm taken at IRAM (those marked [a] were taken using a 24-arcsec beam at SEST), and in an 18-arcsec beam at 1100, 800 and 450 μm taken at JCMT. Errors quoted are the statistical 1σ errors on the measurements. Absolute errors are greater than this (see Section 2). Upper limits are 3σ.

Source	BM position		Continuum position		Flux densities			
	RA (1950)	Dec. (1950)	RA (1950)	Dec. (1950)	1300 μm	1100 μm	800 μm	450 μm
L1498	$04^h07^m50.0^s$	+25°02′13″	$04^h07^m50.0^s$	+25°02′31″	10±2.5	35±6	120±18	700±80
L1495D	$04^h11^m12.5^s$	+28°08′20″	$04^h11^m15.5^s$	+28°07′20″	<30	<44	<135	–
L1506	$04^h15^m29.0^s$	+25°12′10″	$04^h15^m30.3^s$	+25°13′22″	–	<48	<66	–
L1521A	$04^h23^m40.0^s$	+26°09′05″	$04^h23^m38.4^s$	+26°09′27″	–	<80	<110	–
L1517C	$04^h51^m35.9^s$	+30°30′00″	$04^h51^m35.9^s$	+30°30′00″	<7.5	<83	100±20	836±160
L1517A	$04^h51^m54.8^s$	+30°28′53″	$04^h51^m54.8^s$	+30°28′53″	<5.4	<60	105±18	1280±330
L1517D	$04^h52^m36.5^s$	+30°34′02″	$04^h52^m36.5^s$	+30°34′02″	–	<130	<120	<4500
L1512	$05^h00^m54.4^s$	+32°39′00″	$05^h00^m54.4^s$	+32°39′37″	<16	45±9	107±21	<6000
L1544	$05^h01^m14.0^s$	+25°07′00″	$05^h01^m13.1^s$	+25°06′36″	46±4	193±30	450±58	1300±240
L1582A	$05^h29^m11.9^s$	+12°28′20″	$05^h29^m14.6^s$	+12°28′08″	<30	<54	160±27	<1240
L134A	$15^h50^m58.1^s$	−04°26′36″	$15^h51^m05.6^s$	−04°26′10″	<163[a]	–	<60	–
L183	$15^h51^m35.7^s$	−02°40′54″	$15^h51^m32.7^s$	−02°42′19″	<134[a]	108±26	269±30	<1500
L1696A	$16^h25^m30.0^s$	−24°12′32″	$16^h25^m30.0^s$	−24°13′22″	<58[a]	62±12	105±18	800±160
L1689A	$16^h29^m10.0^s$	−24°56′32″	$16^h29^m10.5^s$	−24°57′22″	54±15[a]	<102	290±45	2200±300
L1689B	$16^h31^m40.0^s$	−24°30′00″	$16^h31^m47.0^s$	−24°31′45″	134±11[a]	140±34	362±40	<3000
L63	$16^h47^m21.0^s$	−18°01′00″	$16^h47^m19.4^s$	−18°01′16″	<96[a]	<93	367±23	1600±200
B133	$19^h03^m25.3^s$	−06°57′20″	$19^h03^m27.3^s$	−06°57′00″	<56[a]	<120	341±63	<1800

scheme was devised which entailed mapping with JCMT the central region of each core in $^{13}CO(2\rightarrow1)$, giving a resolution of ~20 arcsec. In most cases this revealed one or more peak positions, which were subsequently used for the continuum photometry. It was later found possible to map some of the cores in the continuum, and slight offsets were found in some cases between the ^{13}CO peaks and the continuum peaks. In the case of the remaining continuum observations, even if they are not exactly on peak positions, they are at least close to peaks, since off-peak checks were performed to show that other nearby positions were of lower intensity, or were undetected.

The problem with this approach (the only method possible in the time available) is that it assumes that the cores are optically thin in ^{13}CO, and therefore that peaks of ^{13}CO are true column density peaks within the clouds. This may not be a valid assumption, although the weakness of the $^{13}CO(2\rightarrow1)$ line in all cases (typically $T_{R*} \simeq 0.5$–3 K) rendered attempts at mapping large areas in a more optically thin line equally impractical.

However, in no core was more than one continuum peak found, no matter how many ^{13}CO peaks there were. The other ^{13}CO peaks were all tested for continuum emission, and 3σ upper limits could be placed of order 60–100 mJy at 800 μm (depending upon conditions) for all other ^{13}CO peaks – i.e. less than the weakest peak that was detected. Thus the single peak in each cloud at which we did detect continuum emission is clearly different from the other ^{13}CO peaks. Because dust emission is generally optically thin at submillimetre wavelengths, we claim that the continuum peaks represent true column density peaks within the molecular clouds. Since the ^{13}CO morphology does not suggest larger geometrical cloud depths towards these continuum peaks, it is probable that they correspond to density peaks. It is still possible that other continuum peaks are located within the cores at other positions, but the telescope time required to prove or disprove this will only become feasible with the advent of large submillimetre bolometer arrays.

Figs 1(a)–(f) show ^{13}CO maps of six of the cores – L1506, L1544, L1582A, L1696A, L1689A and L1689B. The origin of each map is at the BM position, although the peak ^{13}CO positions are all offset slightly from the BM positions. This is partly due to the higher resolution of our ^{13}CO data. However, in some cases this may also be partly due to a real offset between the two chemical tracers. All of the cores show structured, non-spherically symmetric morphologies, with either some form of elongation, or double or multiple peaks. This tends to agree with the findings of Myers et al. (1991) that the cores do not generally show spherical morphologies.

However, for 17 of the 21 cores which we have so far studied, we managed to ascertain a peak position, and in most cases more than one ^{13}CO peak. The remaining four sources (L1495B, L1400G, L1400K and L1523) were simply too flat-topped and extended to determine a peak. This either means that these four sources are too extended and amorphous to contain any central condensations, or it may be that they are simply completely optically thick in ^{13}CO, or obscured behind colder ambient material.

Table 1 lists the 17 sources for which we found a ^{13}CO peak. Column 1 lists the source name (we have followed the nomenclature of BM and references therein); columns 2 and 3 list the RA (1950) and Dec. (1950) of the BM position; columns 4 and 5 list the positions at which continuum photometry was performed.

We performed deep-integration continuum photometry of every ^{13}CO peak position within each of the 17 cores that had one or more identifiable ^{13}CO peaks. However, in all cases, we only detected continuum emission from one peak within each core. Typical integration times varied from 5 min to ~1–2 h, depending upon the conditions. The observations were carried out as a series of pairs of 10-s integrations. The source is first

placed in the left-hand beam of the telescope, while chopping the secondary mirror by 150 arcsec in azimuth at 7.8 Hz, and the mean difference 'left–right' is calculated, along with the standard deviation and signal-to-noise ratio. The telescope is then 'nodded' to put the source in the right-hand beam and the difference 'right–left', along with standard deviation and signal-to-noise ratio, is calculated. The mean of the pair of measurements is then stored, and the running mean and standard deviation are calculated throughout the integration, and finally also stored to file.

If the sky appeared to be unstable then several such integrations were carried out, and monitoring of the secondary calibrators was performed between each integration. Finally, the mean and standard deviation of all integrations of each source in a single waveband were calculated. If the measurement was at the level of 3σ or less, it was deemed only an upper limit. Measurements above the level of 5σ were deemed detections (see below).

Table 1, columns 6–9, lists the flux densities of the 17 cores without *IRAS* sources for which we found a ^{13}CO peak, at 1300 μm in a 12- or 24-arcsec beam, and at 1100, 800 and 450 μm in an 18-arcsec beam. 12 of the 17 sources have detections at one or more wavelengths, while the remaining five have only upper limits. It can be seen, by comparison with the flux densities quoted by Ladd et al. (1991a) for cores with *IRAS* sources, that the flux densities of cores with *IRAS* sources are greater than those of cores without *IRAS* sources.

The errors quoted in Table 1 are the 1σ errors, calculated as described above, to show that the detections are all at least 5σ, except for L1498 and L1689A at 1300 μm, L183 and L1689B at 1100 μm and L1517A at 450 μm, which are all between 4 and 5σ. However, since these all have 5σ detections at other wavelengths, their identification is believed to be secure. Note that the absolute calibration errors are greater than this, as described in Section 2. The upper limits listed are all 3σ limits.

As well as the photometry listed in Table 1, we attempted 350-μm measurements of L1498 on the evenings of 1991 December 30 and 31, and obtained a 3σ upper limit to its flux density of 1.2 Jy. We also attempted 350-μm photometry on the mornings of 1993 March 4–7 and obtained a detection of L1689A at 4.1 ± 0.7 Jy, a marginal detection of L63 at 1.4 ± 0.3 Jy, and 3σ upper limits for L183 of <1.9 Jy and L1689B of <7.5 Jy. We estimate the absolute calibration uncertainty to be ~40–50 per cent at 350 μm.

We compared the detection rate in Table 1 with that of the NH_3 observations of BM and found that, for 16 of the 17 cores, if the core was detected by BM then we detected it in the submillimetre continuum. If, however, the core was not detected in NH_3 by BM then we did not detect it in the submillimetre continuum. This exact correlation is only marred by one exception, which is L134A. This core was detected by BM in NH_3, but was not detected by us. None the less, this level of agreement shows that the submillimetre continuum is virtually as reliable as NH_3 in tracing dense cores in dark clouds. In contrast, there is no correlation between the existence of ^{13}CO clumps and the detection of NH_3. Of the four cores that showed no appreciable structure in ^{13}CO, two had NH_3 detections and two did not.

Figs 2(a)–(e) show submillimetre 800-μm continuum isophotal contour maps of the five sources for which time and conditions permitted mapping to be carried out – L183, L1689A, L1689B, L63 and B133. Note that the origins of the maps in Fig. 2 are the continuum positions listed in Table 1, and so are different from those in Fig. 1, and that the continuum peaks are close to, but not exactly coincident with, the ^{13}CO peaks. This is presumably an effect of the ^{13}CO not being completely optically thin. Note also that, although most cores contain more than one ^{13}CO peak, none of the cores contains more than one continuum peak.

These objects are the faintest so far mapped in the continuum by JCMT, and required long integration times of 5 min per point, together with a point-by-point step-mapping technique, at a sampling rate of 20 arcsec, rather than the usual on-the-fly mapping technique used by JCMT. Hence the maps are undersampled, and it was not possible to map all cores out to the background cloud. The maps illustrate how well peaked these sources are, with FWHM of the order of 1 arcmin, and they show that, for these sources at least, the positions for which photometry was obtained are true continuum emission peaks.

The value of the continuum flux density at the point in each continuum map that corresponds to the ^{13}CO peak varies from 25 per cent of the peak continuum flux density (L1689B) to 80 per cent (L63), with a mean of ~50 per cent. Assuming a similar result for those cores that were not mapped, we conclude that the detections without maps quoted in Table 1 may similarly be underestimated by up to a factor of two.

The 800-μm maps were all made using a 150-arcsec chop throw, and so are insensitive to structure on scales larger than this. This means that the structures seen are true peaks, and the flux densities measured are of the clumps themselves, and not the more diffuse emission from the background cloud in which they are embedded. Furthermore, the observed extent of each source is significantly less than the chop throw, which suggests that the extent we have observed corresponds to the actual physical size of the source, and indicates that the sources are not scale-free, but have definite edges. In the case of L1689B, this view is further supported by the fact that a quick, independent, five-point map obtained at SEST, with a different beamsize and chop throw, yielded results consistent with the size measured at JCMT (20 arcsec from the centre, the average signal measured at SEST was ~80 per cent of the peak flux density). The different properties and parameters that can be derived from these data will now be discussed.

4 DATA ANALYSIS

4.1 Source sizes

Table 2 lists the derived parameters of the cores that were mapped in the continuum. Column 1 gives the source name, column 2 lists the assumed distance to the source (MLB), and columns 3 and 4 detail the (undeconvolved) FWHM of the major and minor axes of the continuum emission from the cores seen in Fig. 2, in arcsec and parsec. B133 has only one FWHM given, since it was not mapped over a sufficiently large area to ascertain its FWHM in two orthogonal directions. All of the clumps appear to show some departure from circular symmetry. Although partially due to the relatively low signal-to-noise ratio of the maps, we think that this systematic asymmetry is at least partly a real effect in the sources themselves.

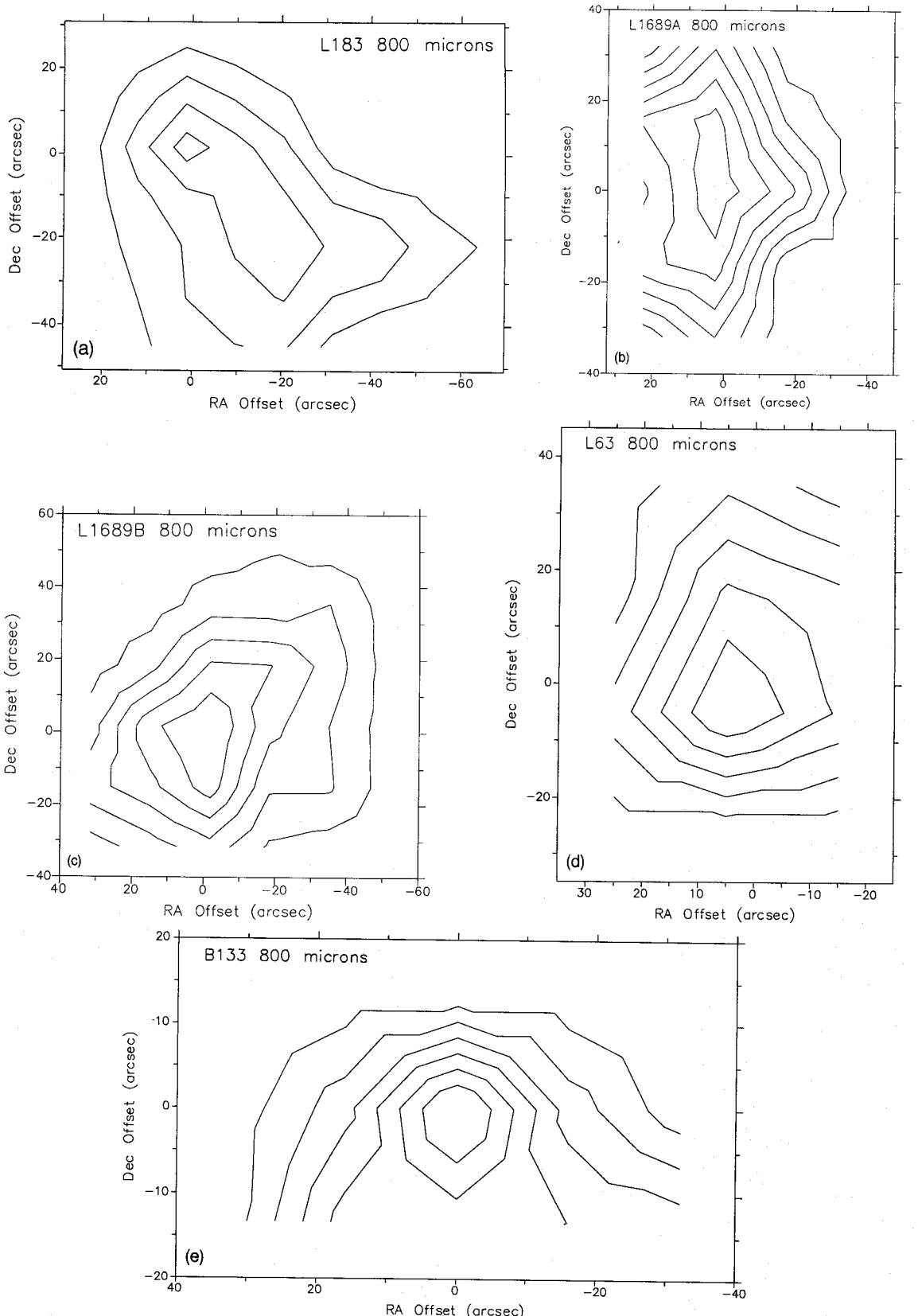

Figure 2. Isophotal contour maps, taken with JCMT, of submillimetre continuum emission from five of the starless cores at 800 μm. RA and Dec. offsets are marked in arcsec. (a) L183, map origin is at RA (1950) = $15^h51^m32^s.7$, Dec. (1950) = $-02°42'19''$, base contour level is 50 mJy beam^{-1}, contour interval is 50 mJy beam^{-1}, mean 1σ noise level is 22 mJy beam^{-1}. (b) L1689A, map origin is at RA (1950) = $16^h29^m10^s.5$, Dec. (1950) = $-24°57'22''$, base contour level is 60 mJy beam^{-1}, contour interval is 40 mJy beam^{-1}, mean 1σ noise level is 37 mJy beam^{-1}. (c) L1689B, map origin is at RA (1950) = $16^h31^m47^s$, Dec. (1950) = $-24°31'45''$, base contour level is 60 mJy beam^{-1}, contour interval is 60 mJy beam^{-1}, mean 1σ noise level is 55 mJy beam^{-1}. (d) L63, map origin is at RA (1950) = $16^h47^m19^s.4$, Dec. (1950) = $-18°01'16''$, base contour level is 160 mJy beam^{-1}, contour interval is 40 mJy beam^{-1}, mean 1σ noise level is 27 mJy beam^{-1}. (e) B133, map origin is at RA (1950) = $19^h03^m27^s.3$, Dec. (1950) = $-06°57'00''$, base contour level is 80 mJy beam^{-1}, contour interval is 40 mJy beam^{-1}, mean 1σ noise level is 53 mJy beam^{-1}.

Table 2. Derived parameters of the cores that were mapped in the continuum. Distances are taken from MLB. FWHM were measured from Fig. 2. Mass estimates use temperatures derived from greybody fits to the flux densities of column 5 (which agree with the temperatures listed by BM). The mean density within the FWHM of each core is quoted in column 10. Luminosities are measured from Fig. 5. Virial masses calculated from MLB velocity dispersions are listed in column 9. The distance to B133 is not known, so a mass, density and luminosity could not be calculated in this case. See text for discussion.

Source	Dist. (pc)	FWHM (arcsec)	FWHM (pc)	$S_{800\mu m}^{FWHM}$ (Jy)	$S_{800\mu m}^{Total}$ (Jy)	T_{gb} (K)	M_{FWHM} ($M_\odot$)	M_{vir} ($M_\odot$)	$n(H_2)$ (cm^{-3})	L_{Tot} ($L_\odot$)
L183	150	60×40	0.044×0.029	1.8	2.8	8^{+4}_{-3}	2.2	0.8	2.0×10^6	0.05–0.2
L1689A	160	60×50	0.047×0.039	1.8	2.7	20^{+5}_{-8}	0.5	3.1	2.4×10^5	1.7–2.25
L1689B	160	60×60	0.047×0.047	3.0	4.2	15^{+3}_{-7}	1.2	1.2	4.7×10^5	0.9–1.8
L63	160	60×45	0.047×0.035	2.4	3.4	8^{+2}_{-3}	3.3	0.8	2.0×10^6	0.15–0.35
B133	–	30	–	0.5	0.8	–	–	–	–	–

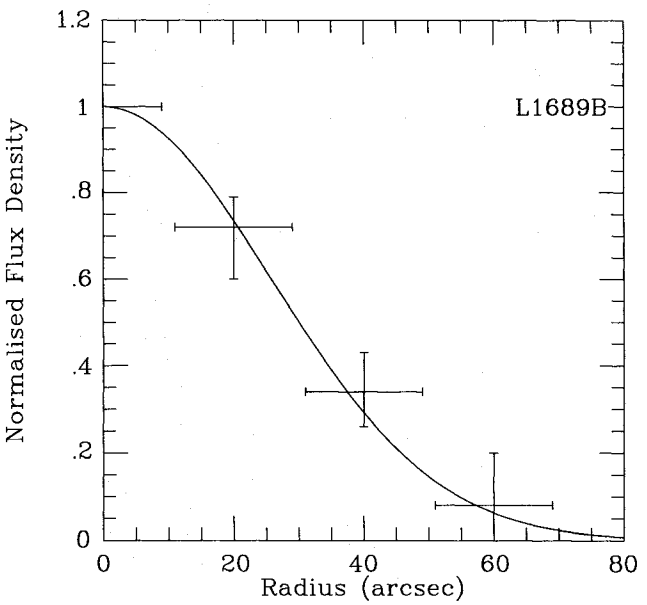

Figure 3. Azimuthally averaged radial flux density profile of L1689B normalized to the peak flux density. The solid line is a Gaussian consistent with the data. See text for discussion.

It can be seen from Table 2 that all of the sources have FWHM significantly greater than the half-power beamwidth of the observations. Measurements of the flux density emitted one full beamwidth from the peak in all cores show the emission at that radius to vary from 50–75 per cent of the peak flux density. For a point source the flux density one beamwidth from the peak should be only 6 per cent of the peak flux density. This shows that all of the sources are clearly spatially resolved.

Four of the five sources have a geometric mean FWHM greater than twice the beamwidth. The exception is B133, for which there was not time to map the entire area. This source also has a less clearly determined distance, and is probably more distant than the others (BM).

These results can be compared with the equivalent parameters for Myers cores with *IRAS* sources. In a survey of cores with *IRAS* sources, Ladd et al. (1991b) found that 24 out of a total of 27 cores have FWHM less than twice the beamwidth. These authors were studying a sample of cores at similar distances to our sample, with similar resolution – they too used JCMT at 800 μm – and so this finding is not a selection or instrumental effect, but a real, physical difference between the two samples. Similarly, the circumstellar structures mapped with IRAM by André & Montmerle (1994) around *IRAS* Class I sources in ρ Oph are also significantly more compact than the starless cores presented here (the DCO^+ results of Loren, Wootten & Wilking (1990) show that most ρ Oph Class I sources are equivalent to Myers cores with *IRAS* sources). Thus cores without *IRAS* sources tend to be more extended than cores with *IRAS* sources.

The flux densities within the FWHM of each of the maps shown in Fig. 2 were measured, and these are listed in Table 2, column 5. Fig. 3 shows a plot of azimuthally averaged flux density versus radius for the map in Fig. 2 that covers the largest area, L1689B, normalized to the peak flux density. The horizontal 'error bars' indicate the FWHM of the beamsize; the vertical 'error bars' represent the total deviation from spherical symmetry observed. The solid line is a Gaussian, which is approximately consistent with the data. Elliptical Gaussians, with FWHM equal to those shown in column 3 of Table 2, were fitted to the data shown in Fig. 2, and the total flux density under each is listed in column 6 of Table 2.

The data in Fig. 3 are not consistent with the emission predicted from a constant-density, constant-temperature finite sphere or ellipsoid, which would appear as a quadrant of an ellipse on Fig. 3. The data show slightly more central condensation than this, and this was found to be true for all of the cores seen in Fig. 2.

Thus we see that the continuum emission from clumps in Myers cores without *IRAS* sources is more spatially extended, and less centrally condensed, than that from cores with *IRAS* sources. However, the cores are more centrally condensed than constant-density ellipsoids. This is fully consistent with the view that cores without *IRAS* sources are at a pre-protostellar stage, and are likely to evolve into cores with *IRAS* sources.

4.2 Radial profiles

Figs 4(a)–(d) show azimuthally averaged radial flux density profiles versus projected radius, θ, for each of the fully mapped cores from Fig. 2, on a log-log scale (B133 is excluded because we did not map a sufficiently large area). All are normalized to their peak flux density. The horizontal 'error bars' indicate the FWHM of the beamsize, to show that each of the data points is completely independent. The vertical 'error bars' represent

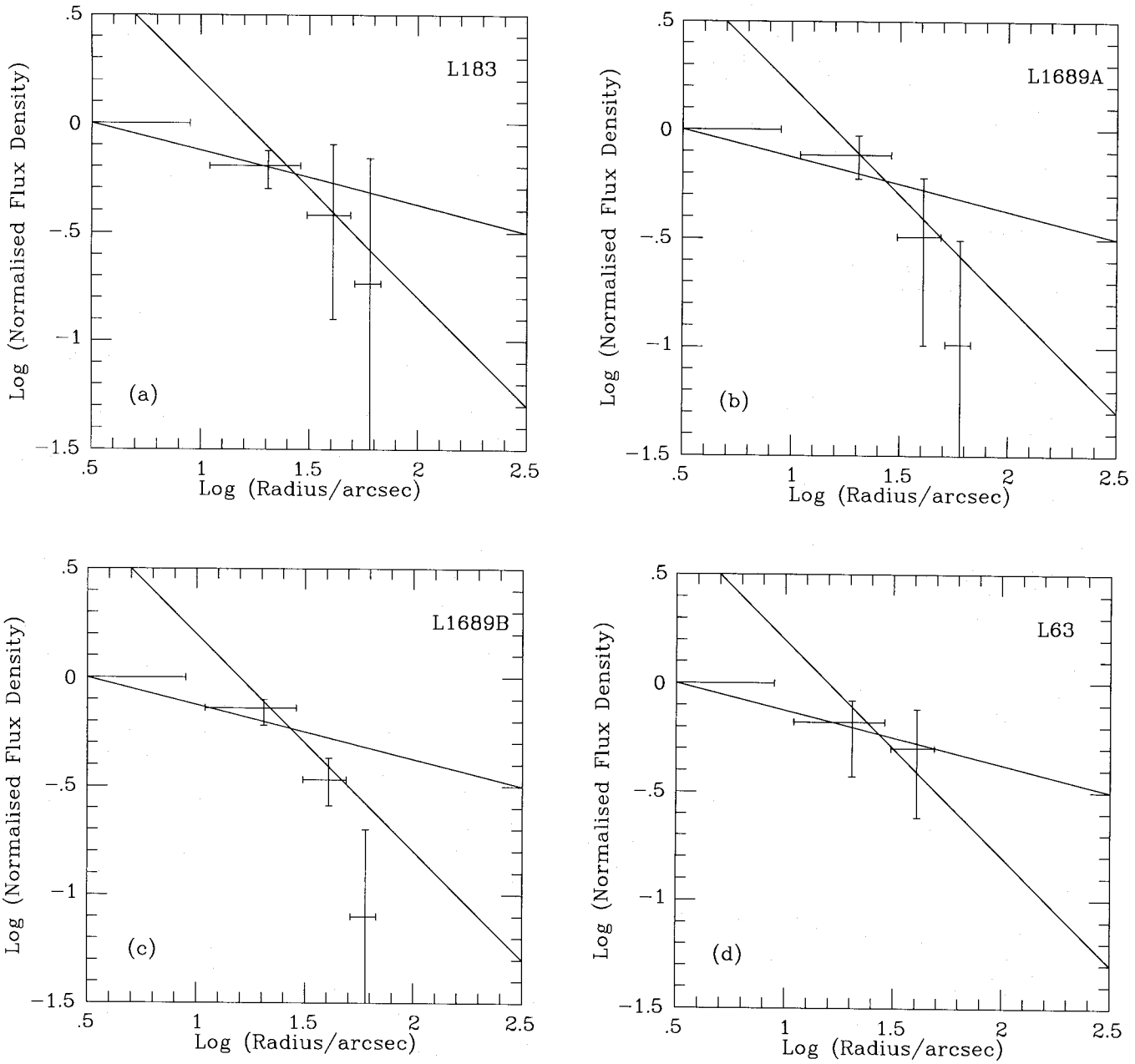

Figure 4. Azimuthally averaged radial flux density profiles of each of the cores that were mapped fully in the continuum, plotted on a log-log scale. The two straight lines plotted on each diagram are power-law radial profiles corresponding to $S_\nu(\theta) \propto \theta^{-1}$ and $S_\nu(\theta) \propto \theta^{-0.25}$ (corresponding to $\rho(r) \propto r^{-2}$ and $\rho(r) \propto r^{-1.25}$). The inner part of each core appears consistent with the flatter profile, while the outer part is consistent with the steeper profile. Contrary to the predictions of the Standard Protostellar Model, no single power law fits all of the data. See text for discussion.

the total deviation from spherical symmetry observed. On a log-log plot a power-law radial flux density profile is simply a straight line. The two solid straight lines shown on each plot correspond to $S_\nu(\theta) \propto \theta^{-1}$ and $S_\nu(\theta) \propto \theta^{-0.25}$.

None of the cores for which four independent data points exist – L183, L1689A and L1689B – is entirely consistent with a single power-law profile throughout its full extent (except L183 at the limit of its 'error bars'). In each case the outer regions (at radii greater than 20 arcsec) are consistent with the θ^{-1} profile, but extrapolation of this profile into the centre overestimates the peak flux density in each case by more than a factor of five. L63 is consistent with the flat $\theta^{-0.25}$ curve through its three data points, and, although its outer two data points are consistent with the θ^{-1} profile, its extrapolation similarly overestimates the peak flux density by a factor of five.

Conversion of two-dimensional radial intensity profiles into three-dimensional radial (r) density profiles requires assumptions about the temperature profile and the geometry. We assume isothermal cores, i.e. that the temperature does not increase towards the centre. This derives from the luminosity arguments, in Section 4.4 below, that the cores are not sufficiently luminous to contain central heating sources (this is further reinforced by the lifetime arguments in Section 5

below). For the sake of simplicity, we also assume spherical geometry.

Standard techniques (for example Casali 1986; Adams 1991) show that if temperature $T(r) \propto r^{-q}$, density $\rho(r) \propto r^{-p}$ and flux density $S_\nu(\theta) \propto \theta^{-m}$ then the indices are related by the simple expression $m = p + q - 1$. In the isothermal case $q = 0$, and thus $p = m + 1$. So we see that the θ^{-1} and $\theta^{-0.25}$ flux density profiles translate into r^{-2} and $r^{-1.25}$ space density profiles.

The Standard Protostellar Model predicts that the precursor cores in which star formation occurs should have a standard isothermal sphere profile of $\rho(r) \propto r^{-2}$ (Shu 1977). This projects into a two-dimensional flux density profile as $S_\nu(\theta) \propto \theta^{-1}$. All cores appear to have radial density profiles flatter than this in their inner regions, and only their edges are satisfactorily fitted by such a steep radial density profile.

It was claimed by Ladd et al. (1991b) that the cores with *IRAS* sources were consistent with the power-law radial density profile predicted by the Standard Protostellar Model. However, study of their fig. 15 shows that, due to the smaller sizes of cores with *IRAS* sources, they did not necessarily have the resolution to rule out a model in which the cores have a steep radial profile in their outer parts, with a flatter profile in their inner regions. Thus the profiles we observe here for starless cores are not inconsistent with those seen in the more evolved cores with *IRAS* sources.

Furthermore, previous molecular line surveys of these cores, which found them to be consistent with the r^{-2} density profile (Myers et al. 1991; Fuller 1992), may similarly be biased by their lower resolution, leaving them sensitive only to the radial profiles in the outer parts of the cores. Thus such surveys would not be able to detect the flattening of the radial density profile in the inner regions, which our higher resolution observations have discovered.

This flattening in the centres of cores suggests either that the cores are not sufficiently evolved to have reached the r^{-2} isothermal sphere density profile yet, or that such a steep profile is never achieved by star-forming cores, due to other processes such as hydromagnetic support. A recent model (Crutcher et al. 1994) predicts radial profiles based on a thermally and magnetically supported cloud. The model is a fully implicit, multifluid, adaptive-grid code that reliably follows both the early, quasi-static, ambipolar-diffusion-controlled phase of core formation and the later, dynamic contraction phase of the thermally and magnetically supercritical core. The initial magnetohydrostatic model has a flat density profile in the core, and an $r^{-1.7}$ profile in the envelope.

As ambipolar diffusion drives the formation of a supercritical core, the radius of the flat core shrinks, with an $r^{-1.5}$ profile in the outer parts of the supercritical core. In the envelope just outside the supercritical core, the index of the density profile becomes greater than 2 as mass is fed into the collapsing core. These magnetically supported models, which predict a break in the radial profile at a certain critical radius, appear to describe our observed radial profiles at least qualitatively. More detailed comparisons with such models will be the subject of future work.

4.3 Spectral energy distributions

Figs 5(a)–(d) show the spectral energy distributions (SEDs) of the four sources with full 800-μm continuum maps. They are shown as plots of $\log(S_\nu)$ versus $\log(\nu)$. The 800-μm flux densities used are the total flux densities listed in column 6 of Table 2. The total flux densities at the other submillimetre wavelengths were calculated by scaling the peak flux densities at all wavelengths listed in Table 1 as if they too were Gaussians of FWHM listed in Table 2.

Approximate upper limits corresponding to *IRAS* non-detections are also shown in Fig. 5. These were obtained by studying the *IRAS* Point Source Catalog (Beichman et al. 1988) and finding nearby sources with upper limits in one or more wavebands. The mean upper limit of the few nearest sources in each waveband was taken to be indicative of the *IRAS* background level in that waveband, and thus a meaningful upper limit for the non-detection of a point source. This could only be improved by detailed study of the raw *IRAS* data in every region.

The solid curve in each diagram is a greybody consistent with the data for each object, of the form $F_\nu = B(\nu, T)(1-e^{-\tau(\nu)})\Omega_s$, where $B(\nu, T)$ is the blackbody function, Ω_s is the solid angle of the emitting source and $\tau(\nu)$ is the optical depth at frequency ν. The form of the optical depth is $\tau(\nu) \propto \nu^\beta$.

The greybody fits were generated in the first instance by using the gas temperature for each source found by MLB. Table 2, column 7, lists the temperature of the greybody, T_{gb}, for each source, and this is thus a derived dust temperature for each source. The errors quoted in Table 2 for the temperature give the maximum variation of temperature permitted by the data in each case. In the cases of L183 and L1689A a greybody fit consistent with the data was found with T_{gb} equal to the gas temperature. MLB do not list a temperature for L63. However, for L1689B a value of T_{gb} 5 K lower than the gas temperature was required to obtain a fit to the data, although the two still agree to within combined errors. All of the fits use a value of $\beta = 2$, except for L63 which formally required $\beta = 3$ to fit the data. However, the data in general do not constrain β very tightly.

Good agreement was found between the JCMT data and SEST data for these objects, indicating that the absolute calibration errors at each telescope are no larger than we have estimated.

4.4 Masses and luminosities

Table 2, column 8, lists the derived mass within the FWHM of each source, from the flux density within the FWHM listed in column 5 of Table 2. The masses were calculated using the formula $M_{gas} = S_\nu D^2 / B(\nu, T)\kappa_\nu$, where S_ν is the measured flux density, D is the distance to the source, $B(\nu, T)$ is the blackbody function at frequency ν and temperature T, and κ_ν is the dust opacity per unit mass column density at frequency ν, which is usually taken to have the form $\kappa_\nu \propto \nu^\beta$. The temperature used in each case was the dust temperature estimated from the greybody fit to the SED of each source, which is, in general, consistent with the gas temperature measured for each core by MLB in NH_3.

The value that should be used for the dust mass opacity, κ_ν, is uncertain. In this paper we have followed Hildebrand (1983) and taken a dust emissivity index of β=2 and a gas to dust mass ratio of 100, and hence a dust absorption coefficient at 800 μm of $\kappa_{800\mu m} \sim 0.01$ cm^2 per g of matter (not just dust). Recent work (Cox & Mezger 1989; Mezger 1990) has shown

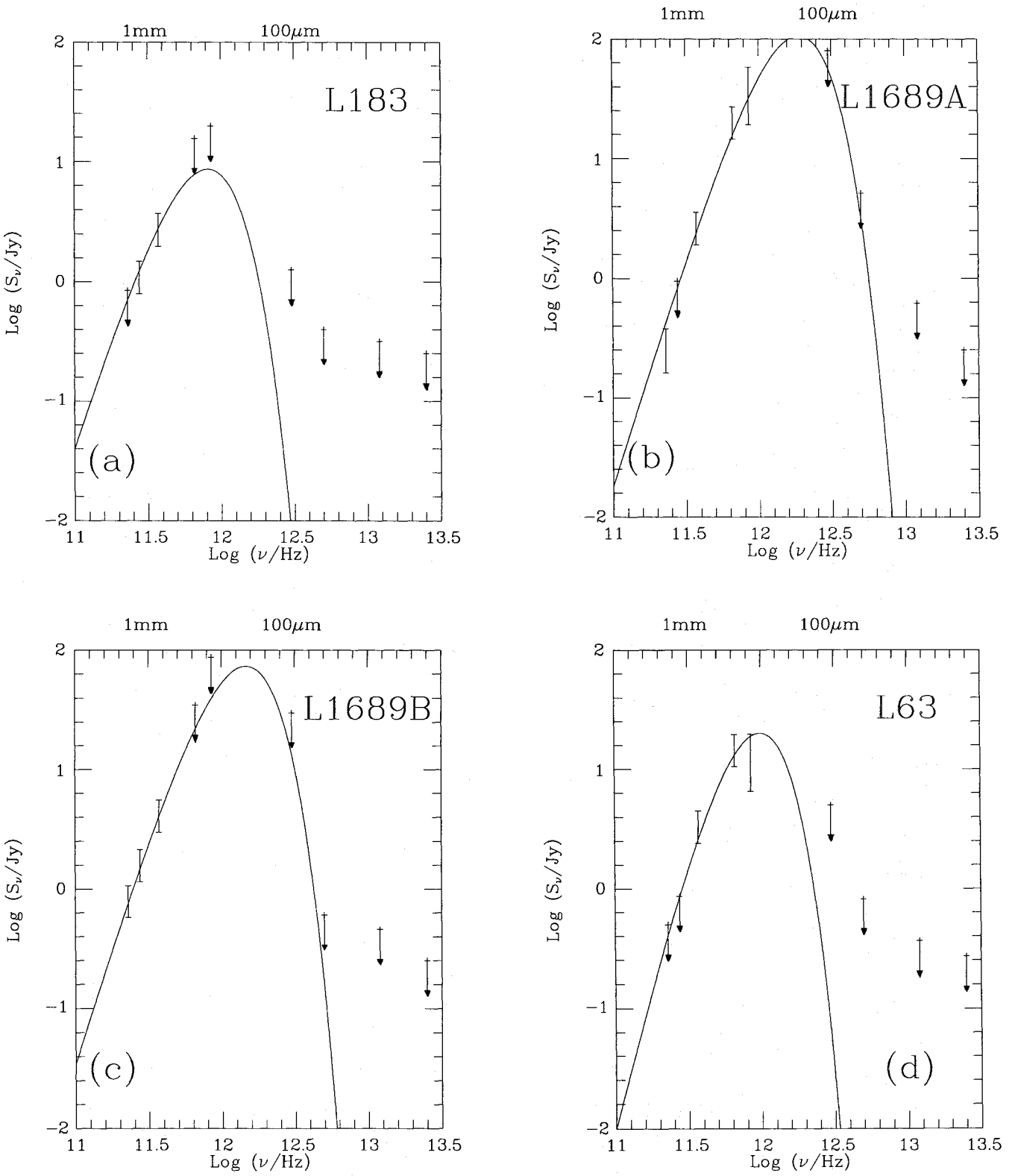

Figure 5. Spectral energy distributions, $\log(S_\nu)$ versus $\log(\nu)$, of the cores that were fully mapped in the continuum. The 800-μm flux densities were measured from the maps of Fig. 2. The flux densities at other submillimetre wavelengths were scaled from the peak flux densities listed in Table 1, using the FWHM of each source listed in Table 2. Upper limits corresponding to non-detections by *IRAS* are also shown. The solid curves are greybodies consistent with the data. The temperature of each of the greybodies is listed in Table 2 along with the range of temperatures consistent with the data.

that the value we use here is appropriate for intermediate-density ($n(H_2)\sim10^5$ cm^{-3}) molecular cloud regions such as these.

In the densest regions ($n(H_2)>10^6$ cm^{-3}), such as ρ Oph A, a value of κ roughly a factor of two higher, following Rengarajan (1984), yielding accordingly lower values of mass, appears to be more appropriate (AWB). In the diffuse ISM ($n(H_2)<10^4$ cm^{-3}) a value of κ a factor of two lower, after Draine & Lee (1984), yielding masses a factor of two higher, seems most apt (Mezger 1990). Thus it can be seen that the uncertainties on the mass estimates due to the dust opacity are about a factor of two. The errors introduced by the uncertainties in the temperature are of similar order, due to the extreme sensitivity of the mass calculation to temperature in these low-temperature regimes.

Table 2, column 10, lists the density within the FWHM of each source, calculated from the FWHM mass in column 8, assuming that the FWHM of each source in the line of sight is equal to the mean of the two FWHM in the plane of the sky. The densities range from $\sim10^5$ to $\sim10^6$ cm^{-3}.

In all cases, the masses we derive for the continuum clumps in Table 2 are lower than the masses derived by MLB for the entire (larger) NH_3 cores. However, the mean density for each continuum clump given in Table 2 is in every case at least an order of magnitude greater than the mean density derived for the whole NH_3 core by MLB. This is consistent with the continuum clumps representing true density peaks within the NH_3 cores. Furthermore, the masses derived for the starless cores are comparable to those found by AWB for SM1 and VLA1623 on the one hand, and greater than the circumstellar masses of Class I sources (André & Montmerle 1994) on the other. This is also consistent with the cores being pre-protostellar in nature.

The luminosities of the sources are listed in Table 2, column 11. The lower limits quoted are measured under each of the greybody curves of Fig. 5, while the upper limits are calculated by treating each of the *IRAS* upper limits as if they were detections. These luminosities are all measured between 12 μm and around 1.3 mm, hence they are far-infrared luminosities. However, since none of these sources has ever been detected at any shorter wavelengths, the luminosities quoted in Table 2 can be considered to be good upper limits to the total luminosity of each source.

The Standard Protostellar Model (ALS and references therein) gives the accretion luminosity of a spherical, non-rotating, non-magnetic protostar as $L_{acc} = GM(t)\dot{M}/R_*$. This equation is simply expressing conservation of energy, by equating the loss of gravitational potential energy with energy radiated. In this equation $\dot{M}$ is the mass accretion rate, which is dependent upon the local sound speed, and is typically $\sim10^{-5}$–10^{-6} M$_\odot$ yr^{-1} (Adams 1991). R_* is the radius of the protostar, which remains roughly constant during accretion at ~3 R$_\odot$ (Stahler, Shu & Taam 1980). Therefore it is possible to calculate the mass that would have already accreted on to the central protostar, from this equation, if the observed cores had entered the protostellar phase.

All of the objects have a luminosity of ≤2 L$_\odot$, which corresponds to a protostar mass of ≤0.02 M$_\odot$, if the luminosity is due solely to accretion. However, this cannot be the case, since at typical accretion rates this would make the age of each protostar only $\sim10^3$–10^4 yr. This is clearly too young, given the number of objects seen (see also Section 5 below), and therefore the cores are probably pre-protostellar in nature, and contain no central condensed source on to which matter is accreting (see also Section 4.5 below). The detected submillimetre emission is consistent with clumps that have cooled to 10–20 K and are heated externally by cosmic rays, nearby stars and the general interstellar radiation field.

In the earliest, isothermal phase of protostellar collapse, the cloud core does not yet contain an opaque stellar object, but nevertheless radiates a 'thermal' luminosity due to the work done by the gravitational forces. This luminosity is easily calculated thermodynamically for any given initial state of the cloud core (Henriksen 1993). In the case of a singular isothermal sphere, one finds $L_{th} = 9(a^5/G)\ln(R_s/R_\circ)$, where a is the isothermal sound speed, R_s is the cloud core radius, and $R_\circ$ is an inner cutoff radius which corresponds to the radius of the future stellar object. With $a = 0.2$ km s^{-1}, $R_s = 10^{17}$ cm and $R_\circ = 10^{11}$ cm, this thermal luminosity is only $L_{th} \approx 1.5\times10^{-3}$ L$_\odot$. Such low values of luminosity are considerably less than that expected from heating by the interstellar radiation field, and hence the cores that we observe are consistent with this early isothermal phase.

4.5 Equilibrium of the cores

The question may be addressed as to whether the clumps within the cores are in virial equilibrium. We can calculate the virial mass for each of the cores, using the linewidths observed by BM and MLB, for comparison with the observed mass, employing the virial relation for velocity dispersion $\sigma = (2GM_{vir}/D)^{0.5}$. The virial masses within the FWHM are listed in column 9 of Table 2. It can be seen that all of the clumps, except L1689A (which has a much larger velocity dispersion than the others), have virial masses lower than or equal to their observed masses. Thus all the clumps appear to be gravitationally bound, and unstable to collapse. However, given the large uncertainties in the mass estimates described above, all that can really be said with confidence is that the cores all have masses consistent with their virial masses, as theoretically expected during the entire ambipolar diffusion phase (e.g., Shu et al. 1993). This is also consistent with the findings of Myers et al. (1991) that the cores are, in general, virialized.

4.6 Individual sources

There is no apparent correlation between any of the observed submillimetre properties of the cores we have studied and the type of cloud in which they are located. BM classified the cores as lying in either globules or clouds, or a mixture of the two. This classification does not appear to have any effect on the parameters we have derived in this paper. However, we have also searched the *IRAS* Faint Source Survey Catalog, FSSC (Moshir et al. 1992), for possible associations with any of the sources listed in Table 1. The FSSC in the Taurus region from 4^h–5^h RA has previously been searched (Beichman, Boulanger & Moshir 1992), and a number of faint sources were found. Cross-checks show that none of our sources was detected by the FSSC in this region. We also searched the FSSC for all the remaining sources in Table 1 and similarly found no matches.

The closest FSSC matches to our observed sources occurred in the cases of L1582A and L63. In the former case F05290+1229 lies only 2.6 arcmin from our discovered source.

This source is relatively bright, with a flux density of 257 Jy at 100 μm. However, it is highly unlikely that this source is our discovered source, given that the 10σ confidence level in the positional accuracy of the FSSC is within 45 arcsec (Moshir et al. 1992). There may be some association between the two sources, perhaps somewhat similar to that between the infrared source S1 and the submillimetre source SM1 (AWB), but proof of this would require further study. The sources F16476-1758 (19 Jy at 100 μm) and F16476-1802 (6.6 Jy at 100 μm) both lie about 5 arcmin from L63, but, by the same arguments, neither of these can be our discovered source. We therefore believe that the upper limits to all of the luminosities quoted in Table 2 are robust.

We also searched the *IRAS* Small Scale Structure Catalog, SSSC (Helou & Walker 1988), for associations with our discovered sources. We found nearby sources in only two cases, L183 and L1544. The source in L183, X1551-028, is some 12 arcmin from our source, with a quoted positional extent of only 3.7 arcmin. Therefore we again discount this as being a different, but possibly related, source. However, in the case of L1544 there is a SSSC source, X0501+251, separated by only 1.1 arcmin from our source, with a positional uncertainty of 5.6 arcmin. Therefore it is likely that these two sources are the same source, or are very closely related. L1544 may therefore be some kind of transitional object between a starless core and a core with an *IRAS* source. The quoted *IRAS* 100-μm flux density of this extended source is 32 Jy, which is clearly larger than an extrapolation of our submillimetre flux densities, so there may be more components to this source than we have discovered. Hence the remainder of this paper will exclude this source from any discussion.

The two most luminous cores that we have discovered are L1689A and L1689B ($\sim$1–2 $L_\odot$), and it may be worth considering whether there is any significance in the observation that they both lie in the same dark cloud (it may for instance simply be due to the higher *IRAS* background in this cloud, which makes the *IRAS* upper limits less constraining on the luminosity). The dark cloud L1689 lies in one of the streamers on the periphery of the Ophiuchus region, and is seen in ^{13}CO to consist of two parts – L1689N and L1689S (Loren 1989). L1689N contains within its boundaries the YSO bipolar outflow source IRAS16293 (Walker et al. 1986), and it also harbours L1689B. However, L1689B is roughly 30 arcmin ($\sim$1.4 pc) from IRAS16293 in a direction totally different from the outflow direction, and the two sources appear to be completely unrelated.

L1689A lies within the L1689S molecular cloud, which also contains the YSO IRAS16288, and the apparent separation between the two sources is only around 8 arcmin ($\sim$0.37 pc). L1689 was mapped in DCO^+ by Loren et al. (1990), who observed dense DCO^+ cores towards the position of the two *IRAS* sources. They saw no detectable emission from either L1689A or L1689B, although their pointing positions were not exactly coincident with either source. However, they did observe an elongation of the DCO^+ core in L1689S in the direction towards L1689A, and it is possible that there is some connection between these two sources. The exact nature of any such connection would require further investigation.

5 EVOLUTION OF THE CORES

It has previously been shown that there are roughly similar numbers of cores with *IRAS* sources as without, and hence that the time-scales of the two phases are similar (Beichman et al. 1986). Roughly one-third of the cores with *IRAS* sources were shown to be associated with T Tauri stars, while the other two-thirds were deduced to be younger objects. The lifetime of a typical Class I source has been estimated to be $\sim 10^5$ yr (Wilking et al. 1989; Kenyon et al. 1990). Embedded Class II sources have the same lifetime as T Tauri stars, i.e., a few times 10^6 yr (e.g., Cohen & Kuhi 1979). The total lifetime for cores with *IRAS* sources is then a few $\times$ 10^6 yr (Beichman et al. 1986). Therefore the total lifetime of a core, from formation of the core to its first containing an *IRAS* source, is also a few $\times 10^6$ yr. The following are simply order-of-magnitude estimates.

We surveyed 20 cores without *IRAS* sources (excluding L1544) and found four (20 per cent) to show no evidence for clumping, or central condensation, on scales less than the FWHM of the core (typically 0.15 pc – BM). The remaining 16 cores (80 per cent) had one or more central condensations or clumps in ^{13}CO. We therefore deduce that a core without an *IRAS* source spends about one-fifth of its lifetime in a roughly uniform state without significant clumping. It then spends four-fifths in a state where it has condensations, but the condensations do not yet contain accreting protostars. An alternative explanation could also be that the cores in which we observed no ^{13}CO clumps are simply optically thick in ^{13}CO.

When we observed the 16 cores (excluding L1544) in the submillimetre continuum, we detected 11 at one or more wavelengths. This is very close to the detection rate of the same sample in NH_3 by BM (they detected 12 of these 16). Thus we deduce that ammonia detections are equivalent to submillimetre continuum detections, and follow the statistics of BM, who found that 50 per cent of all the cores they surveyed, with distances less than 500 pc, were detected in NH_3. This percentage represents an unbiased sample of cores, whereas our source list, when we had determined this one-to-one correlation between NH_3 and the continuum, was skewed towards cores with positive ammonia detections.

Therefore, during that part of its lifetime in which it contains ^{13}CO clumps, a core typically would be expected to spend half of its time in a state where it has not developed a central clump, and then the remaining half with a central clump, detectable in the submillimetre continuum, with density $\sim 10^6$ cm^{-3}. Thus the lifetime of a dense submillimetre clump in the centre of a starless core is $\sim 10^6$ yr.

The fact that none of the cores contains an object like VLA1623 (AWB), which is very bright in the submillimetre but has no *IRAS* source, shows that this phase lasts for no more than roughly one-twentieth of this time, namely $\sim$ 5 $\times$ 10^4 yr. This is consistent with the assertion of AWB that VLA1623 is $<10^4$ yr old. This is also in agreement with Mezger et al. (1992), who surveyed the remainder of the Ophiuchus cloud, and found no more VLA1623-type objects. VLA1623 was classified as 'Class 0' by AWB to signify that it is at an earlier stage of evolution than the typical 'Class I' sources of ALS.

It was suggested that VLA1623 is a true protostar, whose bolometric luminosity of ~ 1 $L_\odot$ corresponds to the accretion luminosity on to a protostar of less than ~ 0.1 $M_\odot$ (AWB). The protostar would then evolve into an object like L1527, which only has *IRAS* detections at the longer wavebands and a bolometric luminosity of 2.1 $L_\odot$ (Ladd et al. 1991a), and would

be designated 'Extreme Class I' (Lada 1991). The luminosity and circumstellar mass of L1527 are consistent with it being an accreting protostar, in which the mass of the protostar is roughly equal to the circumstellar mass (Ladd et al. 1991a; AWB).

The time-scales suggested above for the 'protostellar' phase of VLA1623, evolving into an object like L1527, are in reasonable agreement with predictions of these time-scales from the Standard Protostellar Model (ALS). However, the question raised by this survey is why the clumps appear to exist for so long before collapsing to form protostars at their centres. The free-fall time-scale ($t_{\rm ff} = [3\pi/32G\rho]^{0.5}$) for a clump with mean density $\sim 10^6$ cm^{-3} (found for these cores) is only 5×10^4 yr. It was shown above that the typical lifetimes for the cores observed here are $\sim 10^6$ yr. Therefore the cores cannot be undergoing free-fall collapse. The lifetimes give an indication of either the lifetime of the mechanism(s) that prevents collapse, or the time-scale of the mechanism(s) that triggers collapse.

The Standard Protostellar Model predicts that collapse occurs after turbulent magnetic support of the cores is lost through ambipolar diffusion (Shu, Adams & Lizano 1987, and references therein). Thus it is of interest to calculate the ambipolar diffusion time-scale for a typical clump that we have studied. This is given by $t_{\rm AD} \sim 8t_{\rm dyn}$ (Shu et al. 1987), where $t_{\rm dyn} \sim R_{\rm core}/v_{\rm A}$. Taking $v_{\rm A}$, the Alfvén velocity, to be $\sim \delta v$, the velocity dispersion within a clump ($\sim$0.6 km s^{-1}), after Shu et al., we obtain $t_{\rm AD} \sim 1.3\times10^6$ yr. As already noted by Fuller & Myers (1987), this is consistent with the lifetimes derived for the starless cores.

Thus all of the evidence seems to point to the explanation that the cores we have observed in the submillimetre continuum are magnetically supported, and are undergoing the ambipolar diffusion phase prior to protostellar collapse.

6 CONCLUSIONS

The main findings of this paper are as follows.

(i) A submillimetre continuum survey of Myers cores without *IRAS* sources has revealed the first continuum detections of these 'starless' cores.

(ii) Statistical arguments involving the number of cores that we have detected in the submillimetre continuum, together with their low luminosities, suggest that none of them is a Class 0 accreting protostar like VLA1623.

(iii) For the first time a size difference has been observed between the starless cores and the cores with *IRAS* sources – the starless cores are more extended.

(iv) The radial profiles of the cores are not consistent with a scale-free density distribution. Instead the cores have distinct edges, with FWHM considerably larger than the beamsize.

(v) The data are not consistent with the r^{-2} radial density profile predicted by the Standard Protostellar Model, right into the centres of the cores. Instead the data appear consistent with more recent models of magnetic support of cloud cores, which predict flatter inner profiles for the cores.

(vi) Statistical arguments show that the cores are too long-lived to be undergoing free-fall collapse, and derived masses show the cores to be approximately virialized.

As a result of all of the above findings we conclude that the starless cores that we have detected in the continuum are pre-protostellar in nature, and are currently in the ambipolar diffusion phase prior to protostellar collapse.

ACKNOWLEDGMENTS

The authors would like to thank the JCMT staff of the Joint Astronomy Centre, Hawaii, and the staff of IRAM, Granada, and of SEST, for their assistance while these observations were being carried out. The James Clerk Maxwell Telescope (JCMT) is operated by the Observatories on behalf of the United Kingdom Science and Engineering Research Council (SERC), the Netherlands Organization for Scientific Research (NWO) and the Canadian National Research Council (NRC). Assistance at SEST was also provided by Sylvain Bontemps. Dick Crutcher is thanked for useful input regarding the model for magnetic support of clouds. SERC and the Royal Observatory, Edinburgh, are also acknowledged for Fellowship funding for DWT.

REFERENCES

Adams F. C., 1991, ApJ, 382, 544
Adams F. C., Lada C. J., Shu F. H., 1987, ApJ, 312, 788 (ALS)
André P., Montmerle T., 1994, ApJ, 420, 837
André P., Ward-Thompson D., Barsony M., 1993, ApJ, 406, 122 (AWB)
Beichman C. A., Myers P. C., Emerson J. P., Harris S., Mathieu R., Benson P. J., Jennings R. E., 1986, ApJ, 307, 337
Beichman C. A. et al., 1988, eds, *IRAS* Explanatory Supplement. NASA RP-1190, Washington DC
Beichman C. A., Boulanger F., Moshir M., 1992, ApJ, 386, 248
Benson P. J., Myers P. C., 1989, ApJS, 71, 89 (BM)
Casali M. M., 1986, MNRAS, 223, 341
Chandler C. J., Gear W. K., Sandell G., Hayashi S., Duncan W. D., Griffin M. J., 1990, MNRAS, 243, 330
Chini R., Krugel E., Haslam C. G. T., Kreysa E., Lemke R., Reipurth B., Sievers A., Ward-Thompson D., 1993, A&A, 272, L5
Cohen M., Kuhi L. V., 1979, ApJ, 227, L105
Cox P., Mezger P. G., 1989, A&AR, 1, 49
Crutcher R., Mouschovias T. Ch., Troland T. H., Ciolek E., 1994, ApJ, in press
Davies S. R., Cunningham C. T., Little L. T., Matheson D. N., 1992, Int. J. Infrared Millimeter Waves, 13, 647
Draine B. T., Lee H. M., 1984, ApJ, 285, 89
Duncan W. D., Robson E. I., Ade P. A. R., Griffin M. J., Sandell G., 1990, MNRAS, 243, 126
Fuller G. A., 1992, in Arcoragi J. -P., Bastien P., Pudritz R., eds, Proc. Graduate Workshop, Star Formation. Université de Montreal
Fuller G. A., Myers P. C., 1987, in Scholer M., ed., Physical Processes in Interstellar Clouds. Reidel, Dordrecht, p. 137
Griffin M. J., Orton G. S., 1993, Icarus, 105, 537
Helou G., Walker D. W., 1988, eds, *IRAS* Small Scale Structure Catalog. NASA RP-1190, Washington DC
Henriksen R. N., 1993, in Montmerle T., Lada C. J., Mirabel F., Van Thanh J. T., eds, Proc. XIIIth Rencontres de Moriond, The Cold Universe. Editions Frontières, Gif-sur-Yvette, in press
Hildebrand R. H., 1983, QJRAS, 24, 267
Kenyon S. J., Hartmann L. W., Strom K. M., Strom S. E., 1990, AJ, 99, 869
Lada C. J., 1991, in Lada C. J., Kylafis N. D., eds, The Physics of Star Formation and Early Stellar Evolution. Kluwer, Dordrecht, p. 329
Ladd E. F., Adams F. C., Casey S., Davidson J. A., Fuller G. A., Harper D. A., Myers P. C., Padman R., 1991a, ApJ, 366, 203
Ladd E. F., Adams F. C., Casey S., Davidson J. A., Fuller G. A., Harper D.A., Myers P. C., Padman R., 1991b, ApJ, 382, 555

Larson R. B., 1969, MNRAS, 145, 271
Loren R. B., 1989, ApJ, 338, 902
Loren R. B., Wootten A., Wilking B. A., 1990, ApJ, 365, 269
Mezger P. G., 1990, in Krelowski J., Papaj J., eds, Physics and Composition of Interstellar Matter. Nicolaus Copernicus University, Torun
Mezger P. G., Sievers A., Zylka R., 1991, in Falgarone E. ed., Proc. IAU Symp. 147, Fragmentation of Molecular Clouds and Star Formation. Reidel, Dordrecht, p. 245
Mezger P. G., Sievers A. W., Zylka R., Haslam C. G. T., Kreysa E., Lemke R., 1992, A&A, 265, 743
Moshir M. et al., 1992, eds, Explanatory Supplement to the *IRAS* Faint Source Survey, Version 2. JPL D-10015 8/92, Jet Propulsion Laboratory, Pasadena
Myers P. C., Benson P. J., 1983, ApJ, 266, 309 (MB)
Myers P. C., Linke C., Benson P. J., 1983, ApJ, 264, 517 (MLB)
Myers P. C., Fuller G. A., Mathieu R. D., Beichman C. A., Benson P. J., Schild R. E., Emerson J. P., 1987, ApJ, 319, 340
Myers P. C., Fuller G. A., Goodman A. A., Benson P. J., 1991, ApJ, 376, 561
Orton G. S., Griffin M. J., Ade P. A. R., Nolt I. G., Radostitz J. V., Robson E. I., Gear W. K., 1986, Icarus, 67, 289
Rengarajan T. N., 1984, A&A, 140, 213
Sandell G., Aspin C., Duncan W. D., Russell A. P. G., Robson E. I., 1991, ApJ, 376, L17
Shu F., 1977, ApJ, 214, 488
Shu F. H., Adams F. C., Lizano S., 1987, ARA&A, 25, 53
Shu F., Najita J., Galli D., Ostriker E., Lizano S., 1993, in Levy E. H., Lunine J., eds, Protostars and Planets III. University of Arizona Press, Tucson, p. 3
Stahler S. W., Fletcher A., 1991, in Palla F., Persi P., Zinnecker H., eds, Mem. Soc. Astron. Ital. 62, Young Star Clusters and Early Stellar Evolution. Soc. Astron. Ital., Florence, p. 767
Stahler S. W., Shu F. H., Taam R. E., 1980, ApJ, 241, 637
Thum C. et al., 1992, IRAM Working Report No. 212/92
Walker C. K., Lada C. J., Young E. T., Maloney P. R., Wilking B. A., 1986, ApJ, 309, L47
Walker C. K., Adams F. C., Lada C. J., 1990, ApJ, 349, 515
Ward-Thompson D., Robson E. I., Whittet D. C. B., Gordon M. A., Walther D. M., Duncan W. D., 1989, MNRAS, 241, 119
Wilking B. A., Lada C. J., Young E. T., 1989, ApJ, 340, 823
Zhou S., Evans N., Kompe C., Walmsley C., 1993, ApJ, 404, 232

This paper has been produced using the Blackwell Scientific Publications LaTeX style file.